complete and predicted to be functional VSGs for the Lister427 strain (*1*), although the VSG repertoire for the EATRO1125 strain has not been fully elucidated]. The 65 to 135 VSGs observed before day 30 could represent up to 35% of the preexisting repertoire. Given the sampling frequency in our experiment, these values almost certainly underestimate the expressed VSG diversity in vivo. Therefore, much of the intact VSG repertoire is likely to have been expended early in an infection, as a result of expression and subsequent recognition by the immune system. As a result, the preexisting repertoire of complete VSGs would appear to be insufficient to support the sometimes years-long infections observed in the field. Although parasitemia is much lower in natural hosts, preexisting immunity is common in native mammals (*22*), requiring constant VSG diversification to sustain infection.

Segmental gene conversion events have been demonstrated in both *Trypanosoma equiperdum* and *T. brucei* infections (*7*, *23*, *24*) generating "mosaic" VSGs that were not previously encoded in the genome. Previous studies had noted that mosaics tend to arise later in infection but have not determined when these variants are formed within the genome, or how. It is unknown whether mosaic VSGs form at the active expression site or within the silent repertoire before expression. To identify possible mosaics, we compared expressed VSG sequences to two independently assembled genomes for this parasite strain. Because of limitations in the amount of material available at each time point, we could choose only a few candidates for validation. To test that these were true mosaics and to determine when they formed within the genome, we used VSG-specific primers to confirm their absence from the genome of the parental strain and presence within genomic DNA (gDNA) collected during infection. We identified three mosaic VSGs using this approach. In each case, the mosaic VSG was only detectable by means of polymerase chain reaction (PCR) when it was also being expressed within the parasite population. This suggests that mosaic formation occurs, at least in these cases, shortly before expression, with subsequent transposition into the active expression site, or directly within the active expression site (Fig. 4 and fig. S3). Mosaic formation may be a mechanism for increasing repertoire diversity as infection progresses.

Our results indicate that VSG switching does not occur at a rate that we would have expected to be just sufficient for immune evasion, with only a few variants present at any time. This suggests that recombinatorial mechanisms that expand the preexisting VSG repertoire may be critical for sustaining the long infections observed in natural hosts. Recent work on samples collected from sleeping sickness patients shows higher-than-expected VSG diversity (*25*), indicating that complex VSG dynamics are likely to be clinically relevant. Our results provide a foundation for the study of VSG switching and diversification in vivo and demonstrate the potential of high-throughput approaches for studying antigenic variation, in trypanosomes and other parasitic diseases, in naturally infected humans and animals.

REFERENCES AND NOTES

1. G. A. M. Cross, H. S. Kim, B. Wickstead, *Mol. Biochem. Parasitol.* **195**, 59–73 (2014).
2. C. Hertz-Fowler *et al.*, *PLOS ONE* **3**, e3527 (2008).
3. R. Ross, D. Thomson, *Proc. R. Soc. London Ser. B* **82**, 411–415 (1910).
4. C. M. Turner, J. D. Barry, *Parasitology* **99**, 67–75 (1989).
5. C. M. Turner, *FEMS Microbiol. Lett.* **153**, 227–231 (1997).
6. E. N. Miller, M. J. Turner, *Parasitology* **82**, 63–80 (1981).
7. J. P. J. Hall, H. Wang, J. D. Barry, *PLOS Pathog.* **9**, e1003502 (2013).
8. L. J. Morrison, P. Majiwa, A. F. Read, J. D. Barry, *Int. J. Parasitol.* **35**, 961–972 (2005).
9. K. A. Lythgoe, L. J. Morrison, A. F. Read, J. D. Barry, *Proc. Natl. Acad. Sci. U.S.A.* **104**, 8095–8100 (2007).
10. P. MacGregor, N. J. Savill, D. Hall, K. R. Matthews, *Cell Host Microbe* **9**, 310–318 (2011).
11. S. A. Frank, *Proc. Biol. Sci.* **266**, 1397–1401 (1999).
12. E. Gjini, D. T. Haydon, J. D. Barry, C. A. Cobbold, *Proc. Biol. Sci.* **280**, 20122129–20122129 (2013).
13. M. G. Grabherr *et al.*, *Nat. Biotechnol.* **29**, 644–652 (2011).
14. N. Van Meirvenne, P. G. Janssens, E. Magnus, *Ann. Soc. Belg. Med. Trop.* **55**, 1–23 (1975).
15. F. Claes *et al.*, *PLOS Negl. Trop. Dis.* **3**, e486 (2009).
16. J. R. Seed, *J. Protozool.* **25**, 526–529 (1978).
17. A. R. Gray, *J. Gen. Microbiol.* **41**, 195–214 (1965).
18. J. Lu *et al.*, *Mol. Immunol.* **57**, 274–283 (2014).
19. P. J. Myler, A. L. Allen, N. Agabian, K. Stuart, *Infect. Immun.* **47**, 684–690 (1985).
20. A. Y. Liu, P. A. Michels, A. Bernards, P. Borst, *J. Mol. Biol.* **182**, 383–396 (1985).
21. M. Berriman *et al.*, *Science* **309**, 416–422 (2005).
22. L. Marcello, J. D. Barry, *J. Eukaryot. Microbiol.* **54**, 14–17 (2007).
23. S. M. Kamper, A. F. Barbet, *Mol. Biochem. Parasitol.* **53**, 33–44 (1992).
24. C. Roth, F. Bringaud, R. E. Layden, T. Baltz, H. Eisen, *Proc. Natl. Acad. Sci. U.S.A.* **86**, 9375–9379 (1989).
25. B. A. Eyford, R. Ahmad, J. C. Enyaru, S. A. Carr, T. W. Pearson, *PLOS ONE* **8**, e71463 (2013).

ACKNOWLEDGMENTS

We thank A. Ivens, K. Matthews, K. Gunasekera, and I. Roditi for generously sharing their independently assembled genome sequences and J. Scott for help with early optimization experiments. The work presented has been supported in part by the NIH/National Institute of Allergy and Infectious Diseases (AI085973) to F.N.P., by an NSF Graduate Research Fellowship (DGE-1325261) to M.R.M., and by a Rockefeller University Women in Science Fellowship to M.R.M. All raw data has been deposited to the National Center for Biotechnology Information's Sequence Read Archive under accession number SRP051697, along with all the methods used to generate the figures.

SUPPLEMENTARY MATERIALS

www.sciencemag.org/content/347/6229/1470/suppl/DC1
Materials and Methods
Figs. S1 to S3
References (*26*–*30*)
Databases S1 to S5

10 December 2014; accepted 19 February 2015
10.1126/science.aaa4502

GEOMICROBIOLOGY

Redox cycling of Fe(II) and Fe(III) in magnetite by Fe-metabolizing bacteria

James M. Byrne,[1]*† Nicole Klueglein,[1]† Carolyn Pearce,[2,3] Kevin M. Rosso,[3] Erwin Appel,[4] Andreas Kappler[1]

Microorganisms are a primary control on the redox-induced cycling of iron in the environment. Despite the ability of bacteria to grow using both Fe(II) and Fe(III) bound in solid-phase iron minerals, it is currently unknown whether changing environmental conditions enable the sharing of electrons in mixed-valent iron oxides between bacteria with different metabolisms. We show through magnetic and spectroscopic measurements that the phototrophic Fe(II)-oxidizing bacterium *Rhodopseudomonas palustris* TIE-1 oxidizes magnetite (Fe_3O_4) nanoparticles using light energy. This process is reversible in co-cultures by the anaerobic Fe(III)-reducing bacterium *Geobacter sulfurreducens*. These results demonstrate that Fe ions bound in the highly crystalline mineral magnetite are bioavailable as electron sinks and electron sources under varying environmental conditions, effectively rendering magnetite a naturally occurring battery.

Iron is critical to all living organisms, with many bacteria having developed pathways to access iron either as a nutrient or as an electron acceptor or donor, depending on its mobility, oxidation state, and bioavailability (*1*). Fe(III)-reducing bacteria, including *Geobacter sulfurreducens*, combine reduction of Fe(III) with oxidation of organic matter or H_2 for energy conservation (*2*), whereas phototrophic Fe(II)-oxidizing bacteria such as *Rhodopseudomonas palustris* TIE-1 grow in light with Fe(II) or H_2 as the electron donor (*3*). Bacteria of the *Geobacter* genus and photoferrotrophs have previously been shown to simultaneously occur in sediments (*4*, *5*). The mixed-valent magnetic mineral magnetite (Fe_3O_4), which contains both Fe(II) and Fe(III) in a 1:2 ratio, is often a byproduct of these Fe-metabolization

processes; however, despite its abundance and conductive properties (*6*), the potential use of magnetite in microbial iron and electron cycling is relatively underexplored.

Fe(III)-reducing bacteria readily use dissolved Fe(III) complexes or short-range–ordered minerals (e.g., ferrihydrite) and even magnetite as terminal electron acceptors (*7*–*9*). In contrast, growing cultures of phototrophic Fe(II)-oxidizers are seen to access Fe(II) only in dissolved [$Fe^{2+}_{(aq)}$] or complexed [e.g., Fe(II)-nitrilotriacetic acid] forms (*10*), thus making the bioavailability of magnetite as an electron donor unclear. Nevertheless, *c*-type cytochromes purified from a microaerophilic Fe(II)-oxidizing bacterium can oxidize the surface of magnetite, changing the ratio of iron oxidation states [Fe(II)/Fe(III)] (*11*), and *R. palustris* can accept electrons from a solid electrode (*12*), although direct interaction between living cells and magnetite has not been observed.

We investigated co-cultures of *R. palustris* and *G. sulfurreducens* incubated with magnetite nanoparticles to explore mineral-bound Fe redox cycling. We controlled light and organic matter supply (*13*) in order to investigate the microbially driven mineralogical and magnetic changes that occur within the magnetite due to its dependence on Fe(II)/Fe(III). The magnetite unit cell contains eight Fe(II) and eight Fe(III) octahedrally coordinated ions, which are coupled in antiparallel magnetic orientation to eight Fe(III) tetrahedral coordinated ions. The magnetic moments of the Fe(III) ions cancel one another out, leaving Fe(II) as the main factor in the mineral magnetization. Fe(II)/Fe(III) is based on the total distribution of iron in the formula unit [i.e., in stoichiometric magnetite, Fe(II)/Fe(III) = 0.5]. Indeed, Fe(II)/Fe(III) plays a crucial role in the magnetic properties of magnetite, with maghemite (the fully oxidized form of magnetite) having a lower bulk saturation magnetization (M_s) of ~75 A·m^2/kg (A·m, ampere meter) at room temperature, in comparison to M_s = 92 A·m^2/kg for stoichiometric magnetite (*14*). These experiments support our hypothesis that magnetite can serve as a battery through which bacteria store and withdraw electrons, regulated by changing redox and light conditions.

R. palustris was incubated in constant light with only magnetite (diameter ~12 nm; 10 mg) as an electron donor, leading to a decrease in Fe(II)/Fe(III) (Fig. 1A). After 14 days, Fe(II)/Fe(III) decreased from 0.59 ± 0.03 to 0.31 ± 0.02. Subsequent removal of *R. palustris* and the addition of *G. sulfurreducens* with 10 mM acetate as electron donor initiated magnetite reduction, with Fe(II)/Fe(III) increasing to 0.56 ± 0.02 over 2 days. $Fe^{2+}_{(aq)}$ in the supernatant remained low during oxidation (39 ± 16 μM), but increased to 113 ± 13 μM after *G. sulfurreducens* was added. Sterile controls showed only minor changes in Fe(II)/Fe(III) and $Fe^{2+}_{(aq)}$ over time. Using in situ volume-specific magnetic susceptibility (κ), we analyzed the cultures non-invasively without removing any sample (*15*). Cultures inoculated with *R. palustris* showed a clear decrease in κ by −8.7% (from 1508 ± 9 × 10^{-6} to 1378 ± 7 × 10^{-6} SI) after 9 days (Fig. 1B). κ rapidly increased again (+4.6%) after the addition of *G. sulfurreducens*. After day 10, we observed a decrease in κ, perhaps due to minor magnetite dissolution by *G. sulfurreducens*, as confirmed by a small increase in $Fe^{2+}_{(aq)}$ in the supernatant.

[1]Geomicrobiology, Center for Applied Geosciences, University of Tuebingen, Sigwartstrasse 10, 72076 Tuebingen, Germany. [2]School of Chemistry, University of Manchester, M13 9PL Manchester, UK. [3]Pacific Northwest National Laboratory, Richland, WA 99352, USA. [4]Geophysics, Center for Applied Geosciences, University of Tuebingen, Sigwartstrasse 10, 72076 Tuebingen, Germany.
*Corresponding author. E-mail: James.Byrne@uni-tuebingen.de
†These authors contributed equally to this work.

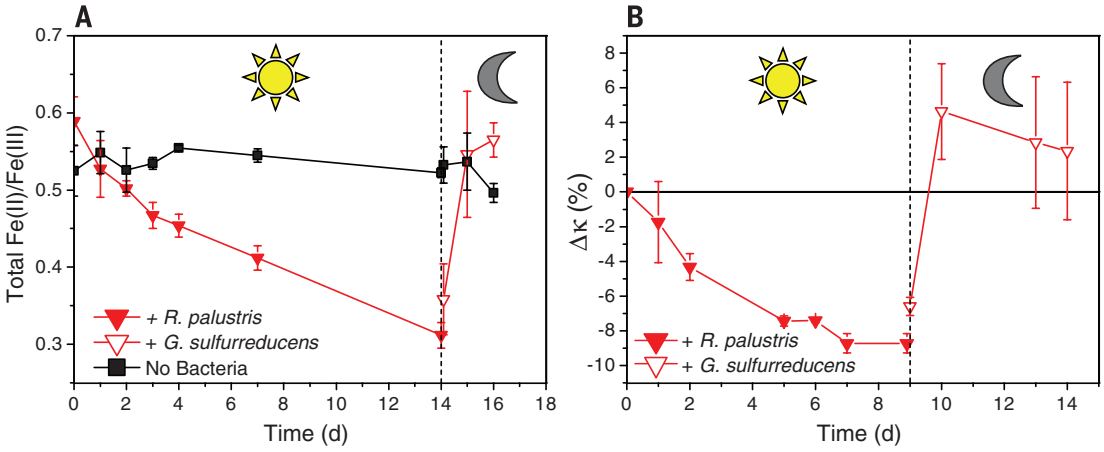

Fig. 1. Oxidation/reduction of magnetite nanoparticles by growing Fe-metabolizing bacteria. (**A**) Observed changes in Fe(II)/Fe(III) over time in magnetite nanoparticles in the presence of Fe-metabolizing bacteria. (**B**) Change in κ with respect to the starting value over time of magnetite nanoparticles in the presence of *R. palustris* and *G. sulfurreducens*. The dashed vertical lines indicate a change from light to dark incubation. Error bars indicate standard deviation of the mean.

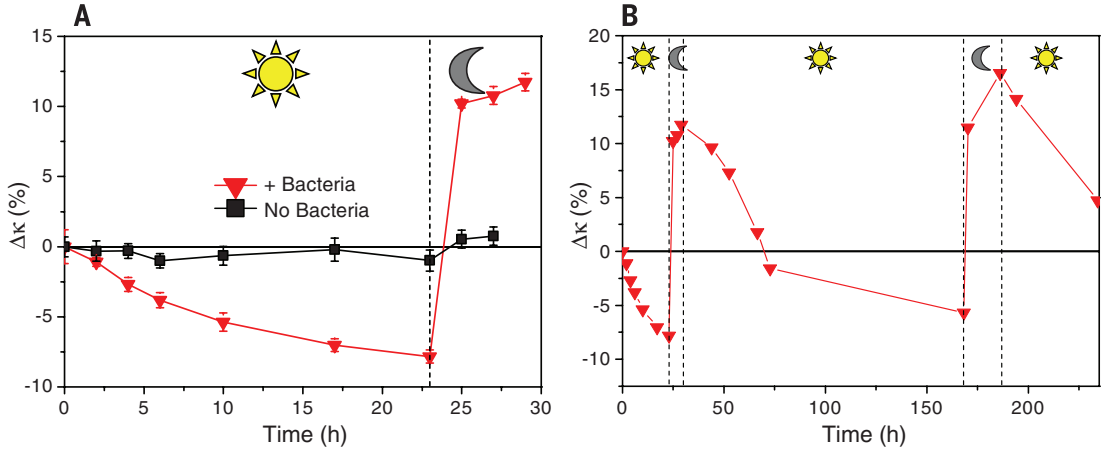

Fig. 2. Magnetite Fe cycling in a cell suspension of Fe-metabolizing bacteria. (**A**) Change in κ of magnetite over 28 hours in the presence of a co-culture of Fe-metabolizing bacteria. Error bars indicate standard deviation of the mean. (**B**) Continuous cycling of magnetite over 240 hours in the co-culture controlled by light and acetate amendment (1 mM).

We examined the consequences of the oxidation/reduction processes on the mineralogical and magnetic properties of the magnetite, using concentrated bacterial cell suspensions of co-cultures of *R. palustris* and *G. sulfurreducens*. These concentrated suspensions enhanced the reaction rate 10-fold, due to a ×10 increase in cell numbers. Over 23 hours in the light, κ decreased by –7.4% (from 1552 ± 13 × 10^{-6} SI to 1437 ± 7 × 10^{-6} SI) due to microbial Fe(II) oxidation by *R. palustris* (Fig. 2A). Without removing the media or Fe(II)-oxidizing bacteria, *G. sulfurreducens* and 1 mM acetate were added to the bottles to stimulate reduction with cultures placed in the dark to inhibit *R. palustris* activity. This stimulated a dramatic increase in κ (+11.7%; $P < 0.05$ at every time point except for $t = 0$ and $t = 2$ for which $P = 0.3$; see Fig. 2). Six hours later, the cultures were returned to light to stimulate *R. palustris*, resulting in κ decreasing by –5.7%. Subsequent acetate addition and incubation in the dark led κ to increase (+16.5%) before decreasing again in the light. Acetate addition without *G. sulfurreducens* (and incubation in the dark) did not affect κ (fig. S1). The concurrent changes in κ show that continuous cycling of iron within magnetite is possible by these bacteria, although the rate of change of κ appears to slow down over repeated cycles, perhaps due to saturation of the magnetite surface with bacteria and/or extracellular organic material (i.e., formation of a biofilm), blocking or at least limiting access to magnetite.

We analyzed the mineralogical properties of the incubated magnetite at three time points, including the starting material (T_{zero}), oxidized magnetite after 23 hours (T_{ox}), and the reduced sample after 6 hours of reduction (T_{red}). Spectrophotometric ferrozine analyses (table S4) showed T_{zero} to be slightly oxidized, with Fe(II)/Fe(III) = 0.45 ± 0.02 as compared to 0.41 ± 0.05 for T_{ox} and 0.52 ± 0.02 for T_{red}, which is comparable to the growth experiment results. Micro–x-ray diffraction (μ-XRD) patterns (fig. S2) showed the characteristic reflections of magnetite without any reflections corresponding to other mineral phases. The average crystallite sizes were calculated as 11.6, 11.6, and 11.5 nm for T_{zero}, T_{ox}, and T_{red}, respectively. Using the lattice parameters (table S4) (*16*), we determined the structural Fe(II)/Fe(III) of T_{zero}, T_{ox}, and T_{red} as 0.47, 0.42, and 0.47, respectively.

^{57}Fe Mössbauer (Fig. 3 and table S1) spectra collected at 295 K show the characteristic overlapping sextets of magnetite corresponding to tetrahedral (A-site) and octahedral (B-site) Fe, with almost no differences between samples and no indication of additional mineral phases. At 140 K, the samples show more pronounced differences. Although the center shifts and hyperfine fields of the A and B sites remained relatively comparable for all samples, the relative populations of each site showed differences,

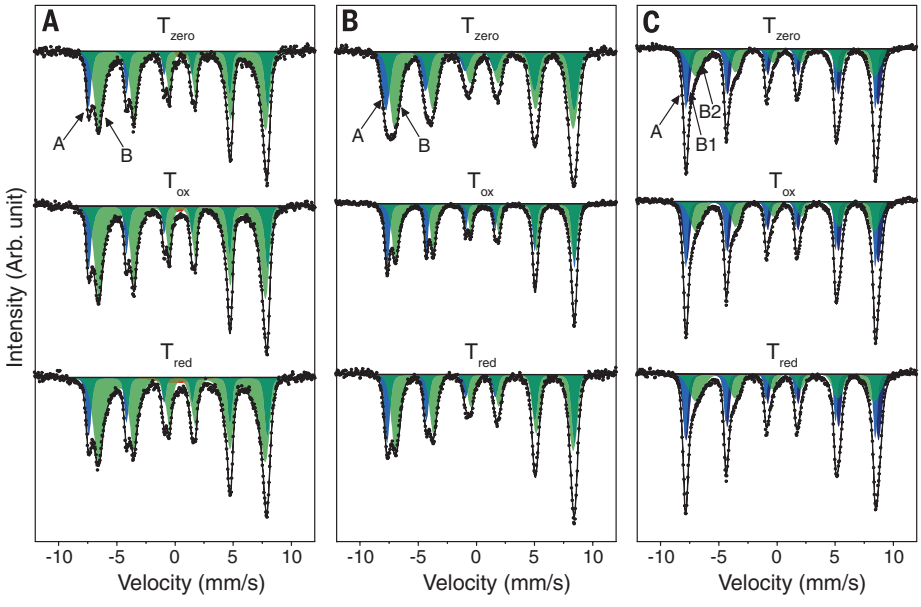

Fig. 3. Mössbauer spectroscopy of magnetite before and after reduction/oxidation. Spectra collected for T_{zero}, T_{ox}, and T_{red} at (**A**) 295 K, (**B**) 140 K, and (**C**) 77 K. All spectra are characteristic of magnetite with tetrahedral (blue) A and octahedral (green) B sites observable at all temperatures.

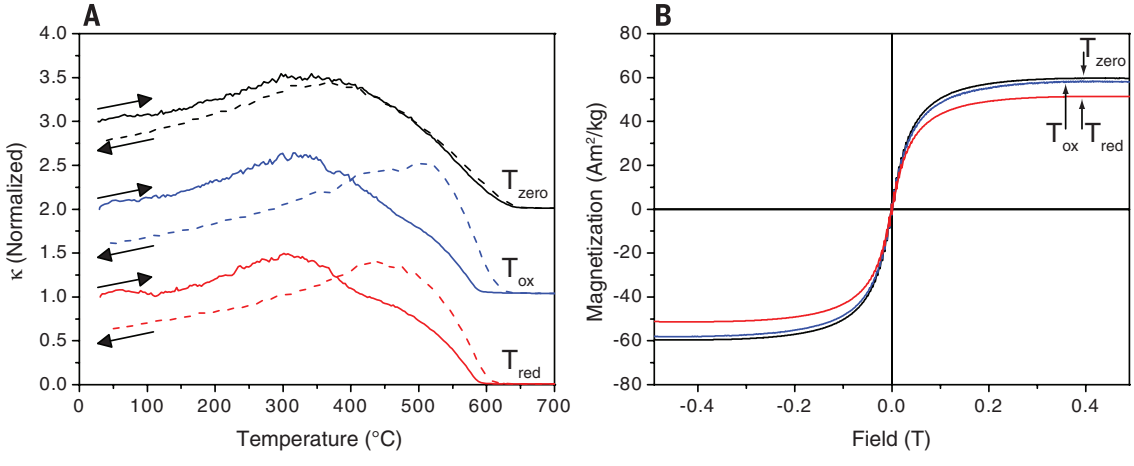

Fig. 4. Magnetic measurements of magnetite before and after reduction/oxidation. (**A**) Normalized high-temperature–dependent susceptibility (κ) curves for T_{zero}, T_{ox}, and T_{red}. Heating curves are shown as solid lines, with dashed lines indicating the cooling curves. Values are normalized to the starting susceptibility measured at the beginning of the heating run and displaced vertically for better comparison. (**B**) Magnetic hysteresis curves collected for T_{zero} (black), T_{ox} (blue), and T_{red} (red) at room temperature.

which were then used to calculate the Fe(II)/Fe(III) for each sample (*17*) (table S4). In accordance with the expected trend, Fe(II)/Fe(III) decreased from 0.46 ± 0.03 (T_{zero}) to 0.42 ± 0.01 (T_{ox}), before increasing to 0.46 ± 0.01 after reduction (T_{red}). At 77 K, the samples were again almost identical with no differences in Fe(II)/Fe(III), although the B site split into two separately ordered subsextets corresponding to Fe^{3+} (B_1) and Fe^{2+} (B_2). The fact that the spectral differences between samples are only observed at 140 K suggests a temperature-dependent effect, probably related to the Verwey transition (T_v ~ 119 K), which can suppressed by magnetite oxidation (*18*).

We also obtained high-temperature magnetic susceptibility (κ-*T*) data for all time points (Fig. 4A). A broad peak with an apex at ~330°C in the heating curve for T_{zero} indicates the presence of single-domain particles or particle clusters that become superparamagnetic at elevated temperatures. κ-*T* decreases to approximately meet the magnetite Curie temperature (T_c ~ 580°C). Apart from a small loss at room temperature (indicating destruction of some magnetite during heating), the cooling curve shows good reversibility. The T_{ox} heating curve looks similar to that of T_{zero}, but in the cooling curve the peak is clearly shifted to a higher temperature. This can be explained by a maghemitized shell that resulted from microbial Fe(II) oxidation that is transformed to hematite during heating due to the thermal instability of maghemite (*19*), leaving behind the magnetite core. The T_{red} heating curve shows similarities to that of T_{ox}; however, the relatively higher κ value at 450°C indicates a higher fraction of magnetite. The loss of susceptibility after cooling for T_{red} is less than for T_{ox} but still obvious; thus, much of the maghemitized volume fraction is obviously still present. The peak in the cooling curve of T_{red} is ~100°C lower than that of T_{ox} but ~100°C higher than that of T_{zero}, suggesting magnetic grain size differences.

Magnetic hysteresis loops (Fig. 4B and table S5) are characteristic of nanoparticulate ferrimagnetic magnetite, with near-zero coercivity (H_c) indicating superparamagnetic (SP) behavior. The saturation magnetization (M_s) of all samples is much lower than the theoretical 92 $A{\cdot}m^2/kg$ of bulk magnetite due to surface spin effects in SP particles (*20*, *21*). The small decrease in M_s of 1.5 $A{\cdot}m^2/kg$ between T_{zero} and T_{ox} is consistent with magnetite oxidation (*22*, *23*). The effect of re-reduction is much less clear, as T_{red} shows an even greater decrease of 8.3 $A{\cdot}m^2/kg$ as compared to T_{zero}. This is counterintuitive to the idea that *G. sulfurreducens* is able to re-reduce the oxidized magnetite to stoichiometric magnetite [i.e., Fe(II)/Fe(III) = 0.5]. One explanation may lie with consideration of the dissolved Fe^{2+} concentration that was detected in the supernatant after the reduction step (127.6 ± 21.2 μM). This dissolution of the particles could in fact have led to an overall decrease in the particle size (as seen from μ-XRD, table S4) leading to the observed decrease in M_s. Alternatively, re-reduction could lead to distortion of the magnetic spin ordering at the surface of the particles; i.e., the maghemitized surface layer is reduced but still forms a distinct shell layer that is not fully coupled to the magnetite core. A nonmagnetic shell in magnetite nanoparticles has previously been shown to form and increases in thickness, depending on the amount of Fe(II) (i.e., level of oxidation) present in the crystal lattice (*24*). Although our average magnetite crystallite size was larger, and therefore a smaller volume fraction was available for oxidation, the formation of a surface layer appears to be the most likely explanation for the impact of bacterial oxidation.

To examine whether our results apply to other systems, we performed further experiments with nitrate-reducing Fe(II)-oxidizing bacteria and other Fe(III)-reducing bacteria (*13*). *Paracoccus denitrificans* strain ATCC 19367, a nitrate-reducing bacterium that is known to indirectly oxidize Fe(II), resulted in a decrease in κ of ~ −10% (from $1885 \pm 81 \times 10^{-6}$ SI to $1693 \pm 49 \times 10^{-6}$ SI) of magnetite (fig. S3). In contrast, *Shewanella oneidensis* MR1, a Fe(III)-reducing bacterium found in anoxic sediments, led to an increase in κ of ~+22% (from $1689 \pm 6 \times 10^{-6}$ SI to $2059 \pm 5 \times 10^{-6}$ SI) (fig. S3). Additionally, the nitrate-reducing bacterium *Acidovorax* sp. BoFeN1 induced a decrease in κ of −8% (from $683 \pm 24 \times 10^{-6}$ SI to $627 \pm 6 \times 10^{-6}$ SI) after 15 days of incubation. This culture was then inoculated with *G. sulfurreducens*, leading to κ increasing to +4.5% ($713 \pm 15 \times 10^{-6}$ SI) (fig. S4), suggesting that the magnetite was re-reduced.

Collectively, these experiments show that magnetite can sustain a vast variety of different bacterial communities functioning as an electron sink, which gets "charged" under reducing conditions by Fe(III) reducers, storing up to 2.6×10^{21} electrons/g (*13*); and then "discharged" under conditions that support its being used as an electron source for Fe(II) oxidizers. In the environment, magnetite could therefore function for microbes as a battery: an environmentally relevant electron sink and source. Alternating oxidation/reduction processes within magnetite could potentially take place in anoxic, photic environments (such as littoral sediments), where environmental fluctuations drive the metabolic use of magnetite (*5*). For example, fluctuating water levels could lead to varying oxygen penetration depths and therefore fluctuating redox conditions, which in turn lead to oxidation and reduction at low and high water levels, respectively. These findings also have direct implications for environmental remediation, in which the reactivity of magnetite with organic contaminants is directly linked to the ratio of Fe(II) to Fe(III) (*25*). Moreover, for environmental magnetic susceptibility measurements, changes in κ are mainly attributed to changes in the amount of magnetite; however, we have shown that microbial activity directly influences the magnetic properties of magnetite without changing the concentration of the mineral. This implies that increasing or decreasing κ could be due to microbial activity rather than magnetite formation, which could have important but currently neglected effects on soil and sediment magnetic properties (*26*).

REFERENCES AND NOTES

1. E. D. Melton, E. D. Swanner, S. Behrens, C. Schmidt, A. Kappler, *Nat. Rev. Microbiol.* **12**, 797–808 (2014).
2. D. R. Lovley, E. J. P. Phillips, D. J. Lonergan, *Appl. Environ. Microbiol.* **55**, 700–706 (1989).
3. Y. Jiao, A. Kappler, L. R. Croal, D. K. Newman, *Appl. Environ. Microbiol.* **71**, 4487–4496 (2005).
4. E. D. Melton, C. Schmidt, S. Behrens, B. Schink, A. Kappler, *Geomicrobiol. J.* **31**, 835–843 (2014).
5. E. D. Melton, C. Schmidt, A. Kappler, *Front. Microbiol.* **3**, 10.3389/fmicb.2012.00197 (2012).
6. S. Kato, K. Hashimoto, K. Watanabe, *Proc. Natl. Acad. Sci. U.S.A.* **109**, 10042–10046 (2012).
7. R. S. Cutting, V. S. Coker, J. W. Fellowes, J. R. Lloyd, D. J. Vaughan, *Geochim. Cosmochim. Acta* **73**, 4004–4022 (2009).
8. H. Dong *et al.*, *Chem. Geol.* **169**, 299–318 (2000).
9. J. A. Smith, D. R. Lovley, P.-L. Tremblay, *Appl. Environ. Microbiol.* **79**, 901–907 (2013).
10. L. J. Bird, V. Bonnefoy, D. K. Newman, *Trends Microbiol.* **19**, 330–340 (2011).
11. J. Liu *et al.*, *J. Am. Chem. Soc.* **135**, 8896–8907 (2013).
12. A. Bose, E. J. Gardel, C. Vidoudez, E. A. Parra, P. R. Girguis, *Nat. Commun.* **5**, 3391 (2014).
13. Materials and methods are available on *Science* Online
14. D. J. Dunlop, Ö. Özdemir, *Rock Magnetism: Fundamentals and Frontiers* (Cambridge Univ. Press, Cambridge, 1997).
15. K. Porsch, U. Dippon, M. L. Rijal, E. Appel, A. Kappler, *Environ. Sci. Technol.* **44**, 3846–3852 (2010).
16. C. I. Pearce *et al.*, *J. Colloid Interface Sci.* **387**, 24–38 (2012).
17. C. A. Gorski, M. M. Scherer, *Am. Mineral.* **95**, 1017–1026 (2010).
18. Ö. Özdemir, D. J. Dunlop, B. M. Moskowitz, *Geophys. Res. Lett.* **20**, 1671–1674 (1993).
19. M. E. Evans, F. Heller, *Environmental Magnetism: Principles and Applications of Enviromagnetics* (Elsevier Science, Academic Press, San Diego, CA, 2003).
20. A. E. Berkowitz *et al.*, *J. Magn. Magn. Mater.* **196–197**, 591–594 (1999).
21. J. M. D. Coey, *Phys. Rev. Lett.* **27**, 1140–1142 (1971).
22. J.-P. Jolivet, E. Tronc, *J. Colloid Interface Sci.* **125**, 688–701 (1988).
23. P. J. Vikesland, A. M. Heathcock, R. L. Rebodos, K. E. Makus, *Environ. Sci. Technol.* **41**, 5277–5283 (2007).
24. R. L. Rebodos, P. J. Vikesland, *Langmuir* **26**, 16745–16753 (2010).
25. C. A. Gorski, M. M. Scherer, *Environ. Sci. Technol.* **43**, 3675–3680 (2009).
26. B. A. Maher, *Elements* **5**, 229–234 (2009).

ACKNOWLEDGMENTS

We thank G. Ojha for help with κ-*T* measurements and C. Berthold for advice on μ-XRD. This work was funded by the Deutsche Forschungsgemeinschaft. Part of this work was funded by the Pacific Northwest National Laboratory Science Focus Area, the Subsurface Biogeochemical Research program of the U.S. Department of Energy Office of Biological and Environmental Research. We thank J. Liu (Peking University) for providing TEM images, which were taken in the Environmental Molecular Science Laboratory (EMSL), a national user facility supported by the OBER and located at PNNL. All data associated with this publication are available at www.pangaea.de.

SUPPLEMENTARY MATERIALS

www.sciencemag.org/content/347/6229/1473/suppl/DC1
Materials and Methods
Figs. S1 to S5
Tables S1 to S5
References (*27*–*34*)

15 December 2014; accepted 20 February 2015
10.1126/science.aaa4834